A DYNAMIC NUCLEATE-BOILING MODEL FOR CO_2 REDUCTION IN INTERNAL COMBUSTION ENGINES

Sergio Bova[1,*], Teresa Castiglione[1], Rocco Piccione[1] and Francesco Pizzonia[1]

[1]DIMEG, Department of Mechanical, Energy and Management Engineering, Università della Calabria, Via P. Bucci, Cubo 44C, 87036 Rende, ITALY

[*]Corresponding author: tel. +39 0984 494828, email address: sergio.bova@unical.it

ABSTRACT

Improvements in cooling system efficiency are required in modern internal combustion engines (ICE). Optimal thermal management presents several advantages in terms of lower pump mechanical power, reduced friction losses and shorter warm-up time, which result in reduced fuel consumptions and CO_2 emissions. These goals can be achieved by adopting lower coolant flow rates, which give rise to nucleate boiling regime. The key requirement for a precision cooling strategy is the capability of developing a reliable, model-based control of the cooling regime. However, there is no model of the cooling system of an SI engine, which identifies precisely the onset of the nucleate boiling. This work fills this void.

This paper presents an original zero-dimensional model of the cooling system of an ICE that predicts dynamically the onset of the nucleate boiling phenomenon and calculates the spatial-averaged metal temperature, the engine-out coolant temperature and the fraction of wall metal area subjected to nucleate boiling. Owing to the little computational effort required, the model is particularly suitable for the development of control algorithms, which can be used to optimize the thermal management strategies in real time and can be easily implemented in the ECU of a modern engine.

The model has been validated by means of experimental tests under several operating conditions, involving variations in coolant flow rate, engine speed and fuel flow rate. The comparison with

experimental data shows a very good agreement. Maximum and average deviation in engine-out coolant temperature are 0.61% and 0.44% respectively under steady-state conditions. The coolant flow rate, which determines the on-set of nuclear boiling computed by the proposed model, is well within the uncertainty range of the experimental evidence.

HIGHLIGHTS

- A 0-D model of nucleate boiling regime for ICE was developed.
- Occurrence and extent of nucleate boiling, coolant and metal temperatures predicted.
- Model predictions assessed by comparison with experimental data.
- Model useful for optimal coolant flow-rate set-up and for quicker engine warm-up.

KEYWORDS

Nucleate boiling; cooling system; dynamic model; internal combustion engines, CO_2 reduction.

NOMENCLATURE

A	engine surface area[m^2]
A_{nb}	part of engine surface involved in nucleate boiling [m^2]
bmep	engine brake mean effective pressure [bar]
c	constant value in Eq.3, 4
C_c	coolant thermal capacity [kJ/K]
C_w	engine thermal capacity [kJ/K]
c_p	specific heat [J/kg K]
c_{pl}	liquid phase specific heat [J/kg K]
E	wall pressure factor
F	convention enhancement factor [-]
FDB	fully developed boiling
h_{fc}	forced convection heat transfer coefficient [W/m^2 K]
h_{lg}	latent heat of vaporization[J/kg]
h_{mac}	macro-convection heat transfer coefficient [W/m^2 K]

h_{mic}	micro-convection heat transfer coefficient [W/m^2 K]
h_{nb}	nucleate boiling heat transfer coefficient [W/m^2 K]
h_{tot}	total heat transfer coefficient [W/m^2 K]
k_l	liquid phase thermal conductivity [W/m K]
L	characteristic length [m]
$\dot{m}_c$	coolant flow rate [kg/s]
$\dot{m}_f$	fuel flow rate [kg/s]
n	exponent in Eq.3[-]
ONB	onset of nucleate boiling
p	pressure [N/m^2]
Pr_l	liquid phase Prandtl number [-]
p_w	wall pressure [N/m^2]
q_{ONB}	nucleate boiling heat flux [W/m^2]
q_w	combustion chamber thermal flux [W/m^2]
$\dot{Q}_c$	thermal power removed by the coolant from the combustion chamber walls[W]
$\dot{Q}_g$	thermal power supplied by the fuel to the combustion chamber walls [W]
$\dot{Q}_r$	thermal power supplied by the coolant to the radiator [W]
Re_l	liquid phase Reynolds number [-]
Re_{2ph}	two phase flow Reynolds number [-]
S	boiling suppression factor [-]
T_c	coolant temperature [K]
$T_{c,r-in}$	coolant temperature at the radiator inlet duct [K]
$T_{c,r-out}$	coolant temperature at the radiator outlet duct [K]
T_{in}	coolant temperature at engine inlet [K]
T_{out}	coolant temperature at engine outlet [K]
T_{sat}	saturation temperature[K]
T_w	engine wall temperature [K]
T_∞	bulk flow temperature [K]
$\dot{V}_c$	coolant volumetric flow rate [dm^3/h]

X	vapour fraction [-]
X	parameter defined in (18) $\left[\frac{K}{\left[W/m^2\right]^{0.5}}\right]$
X_{tt}	Martinelli parameter[-]
ρ_c	coolant density [kg/m^3]
ρ_g	vapour density [kg/m^3]
ρ_l	liquid density [kg/m^3]
μ_g	vapour viscosity [kg/m s]
μ_l	liquid viscosity [kg/m s]
σ	surface tension [N/m]

1. INTRODUCTION

Whereas in the past the focus of regulatory agencies was on the reduction of engine pollutants, today it has moved on to engine fuel consumption, in order to reduce Greenhouse gas (GHG) emission and dependence on fossil fuels. In particular, EU Regulation No 443/2009 (23 April 2009) sets new performance standards to reduce CO_2 emissions from light-duty vehicles, which must reach the 95 g/km limit by 2020 [1], with increasing reduction rates as the deadline approaches. US regulations also demands GHG reductions, even though CO_2 limits similar to the EU ones must be reached 5 years later.

In order to obtain the required CO_2 emission reduction, vehicle manufacturers are developing both alternative powertrain systems (electric vehicles, hybrid electric vehicles, plug-in hybrid electric vehicles) and advanced internal combustion engines technologies [2-3]. Gasoline engines must achieve additional improvements mainly through further downsizing and supercharging boosting, which will push brake mean effective pressure (bmep) towards very high values, up to 25-30 bar [4]. This will place new demands on the engine cooling system, which must be able to remove higher thermal power from reduced surface areas.

In addition to the main contribution of downsizing-turbocharging and other advanced engine technologies, optimized thermal managements and friction reduction will play a significant role in fuel consumption and CO_2 reduction as it is expected to contribute by about 3% to the total CO_2 decrease [4].

The cooling system must, therefore, evolve toward more sophisticated systems. Traditional cooling systems offer a very low possibility of regulation, as the standard mechanical pump is connected to the engine crankshaft, so that the coolant flow rate is fixed by the engine speed. The only regulation possibility relies on the wax thermostat valve, which directs the coolant flow either toward the radiator or toward the pump and, in addition, introduces variable pressure drop to the coolant flow. The heat exchange is dominated by the single-phase forced convection mechanism and circulating mass of coolant and radiator volumes are considerable. This results in a long warm-up process of the engine with higher consumption during the standard driving cycles due to greater lubricants viscosity, non-optimal tolerances and higher friction losses.

The use of an electric pump to substitute the traditional one with generally lower coolant flow rates allows a new degree of freedom of the cooling process control and attains the double goal of lower power consumption by the pump itself and by the engine during the warm-up period. The lower coolant flow rate moves the coolant toward the nucleate boiling regimes, with higher heat fluxes and makes it possible to develop the concepts of precision cooling.

The adoption of a precision cooling strategy offers several advantages over a traditionally cooled engine. The warm-up time can be reduced by about 18%, whereas no drawback was observed on HC emissions and motored friction [5]. In addition a significant reduction of the power required by the water pump (up to 1.85 kW) was estimated [5]. Finally, the use of an electric pump would definitely eliminate the risk of after-boiling, which can happen when an engine is rapidly shut-down after a prolonged period of high load operation [6,7].

Basic research on nucleate boiling has been carried out for several decades [8-11] and the subject is still under investigation [12]. Also the concepts of precision cooling of internal combustion engines and operation under nucleate boiling regimes are not new. Emphasis of first investigations was, however, more on cooling system components than on the heat transfer mechanism. In 1993 Pretscher and Ap [13] conducted an experimental vehicle study in a climate controlled wind-tunnel on the so called "nucleate boiling engine cooling system", by analyzing the performances of circuits components such as condenser, water pump, liquid/vapor-separator, expansion tank, fan control unit. In a following paper Ap and Golm [14] addressed the issue of cost reduction of engine cooling components and proposed the use of a small electric water pump with reduced coolant flow rates, which enabled the occurrence of some nucleate boiling. In 1999 a review of precision engine cooling [15] concluded that cooling systems with low flow rates were promising larger benefits. Subsequent studies addressed the problem of controllability of the cooling system. In 2001 Brace et al [16] proposed a cooling system containing an electric pump and the associated control system, which, however, was based on empirical look-up tables; no attempt was presented to predict or to identify the on-set of nucleate boiling. An attempt to identify experimentally the on-set of nucleate boiling was presented in [17]; an experimental investigation at the test rig was carried-out in order to analyze the behavior of an engine under low coolant flow rate conditions and to identify suitable physical quantities that could be used to detect the on-set of nucleate boiling. However, although it is possible to develop experimental techniques to identify the on-set of the nucleate boiling within a laboratory, this is not practically feasible on-board of a vehicle. The main obstacle to setting up a practical nucleate boiling cooling system is, therefore, the difficulty of obtaining on-board information about the heat transfer regime. This is also associated with the lack of a trustworthy model of the nucleate boiling phenomenon.

This paper presents an original model of the engine cooling system, which is able to detect dynamically the occurrence and the extent of the nucleate boiling phenomenon as well as to calculate the spatial-averaged metal temperature and the engine-out coolant temperature. The model, therefore, makes it possible to run specific control algorithms for managing the cooling process, based on simple on-board transducers. Both the actual wall-to-coolant heat flux and the minimum required heat flux that will produce the on-set of the nucleate boiling are computed and the distance from the two heat fluxes is a useful index for the control strategy. For instance, during engine warm-up, the controller would set the coolant flow rate in order to keep the lowest possible heat transfer coefficient under single-phase flow regime; this guarantees a quicker rise of the engine wall temperature. On the contrary, under fully warmed conditions, based on model predictions, the controller would regulate the coolant flow rate, in order to operate under nucleate boiling conditions and to obtain, as a consequence, the highest possible heat transfer coefficient; this guarantees that only a limited fraction of the wall is subjected to nucleate boiling, thus preserving engine reliability. This work also provides an original and significant contribution to the knowledge of the heat transfer in internal combustion engines and allows the estimation of other key parameters, which cannot be measured directly. Input data needed are engine-in coolant temperature and pressure, coolant mass flow rate, fuel mass flow rate and engine speed. The model was developed by using the Matlab-Simulink® platform, which provides specific tools for implementing software directly on an engine ECU, and was widely validated through test-rig experiments.

2. EXPERIMENTAL SETUP

A small production four-stroke SI engine was used for experimental tests. The engine displaces about 1.2 dm^3 in four in-line cylinders with a four-valve per cylinder aluminum head and about 60 kW between 5000 and 6000 rpm rated power. The test rig was equipped with a Borghi&Saveri FE 260-S eddy current engine torque dynamometer provided with an actuator for remote control of throttle position and with an AVL 733S metering system for engine fuel consumption measurements. A scheme of the engine test-bed and the experimental apparatus is shown in Fig. 1 and the specifications of each measurement device are reported in Table 1.

The cooling circuit was set up with minimal modifications regarding the layout used in a production vehicle, including the heater for car passengers comfort. The standard crankshaft-driven coolant pump, was substituted by a small power electric pump (127 W at 15 V, 2092 dm^3/h maximum flow rate). The standard radiator, used as condenser/radiator, was immersed in a tank filled with water, whose temperature was controlled by means of flowing cool water in order to keep engine inlet coolant temperature constant within a ±1 deg °C error band. A digital PID regulator was used for controlling the cool water flow rate entering in the radiator-tank, providing an output voltage to pilot a solenoid water flow control valve.

Values of the metal temperature of the cylinder block (head gasket side) and cylinder head were measured at various locations (Fig. 2) with k-type thermocouples located in the metal, within a small distance (~1 mm) from the gas/wall interface. The coolant pressure was measured with a miniature piezoresistive pressure transducer, located in the cooling circuit near the engine outlet. Coolant temperatures were measured using PT100-type temperature sensors, installed at the engine inlet and outlet. Coolant volume flow rate was measured using turbine type flowmeters. An optical access was also installed in the cooling circuit near the engine outlet, to observe visually the coolant flow pattern during experimental tests. All tests were performed with a 50/50 (% by mass) mixture of water and commercially available ethylene glycol.

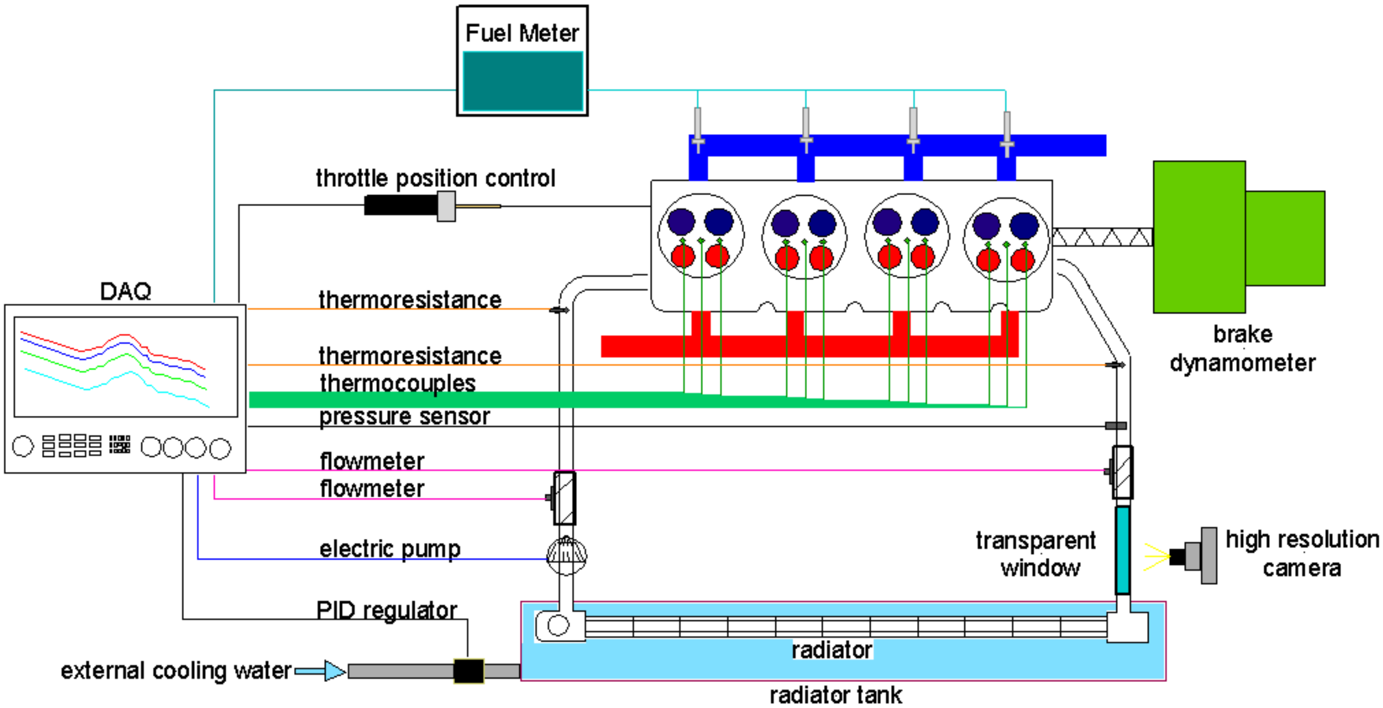

Fig. 1. Schematic of the test rig

Table 1
Main measurement devices specifications

Device type	Model	Specifications
AVL, fuel meter	733 S	FS 150 kg/h Sensitivity and linearity deviation ± 0.12% of the fuel mass withdrawn
BORGHI&SAVERI, eddy current dynamometer	FE 260 S	FS 190 kW @ 12000 rpm Speed measurement: FS 20000 rpm, resolution 1 revolution, accuracy ± revolution Torque measurement: FS 2000 Nm, resolution 1 digit, accuracy ±0.1% FS
EG&G FLOW TECHNOLOGY, flow meter	FT-12	FS 75 l/min Repeatability ±0.05% of reading Linearity ±0.5% over normal
EG&G FLOW TECHNOLOGY, flow meter	FT-16	FS 190 l/min Repeatability ±0.05% of reading Linearity ±0.5% over normal
Pt100 temperature sensor	TRC#P1A1X	FS 120 °C Precision ± 0.15 °C
K-type thermocouples		FS 1000 °C Precision ± 1.5 °C
KULITE, pressure sensor	ETQ-12-375	FS 10 bar Resolution infinitesimal Bandwidth 3kHz

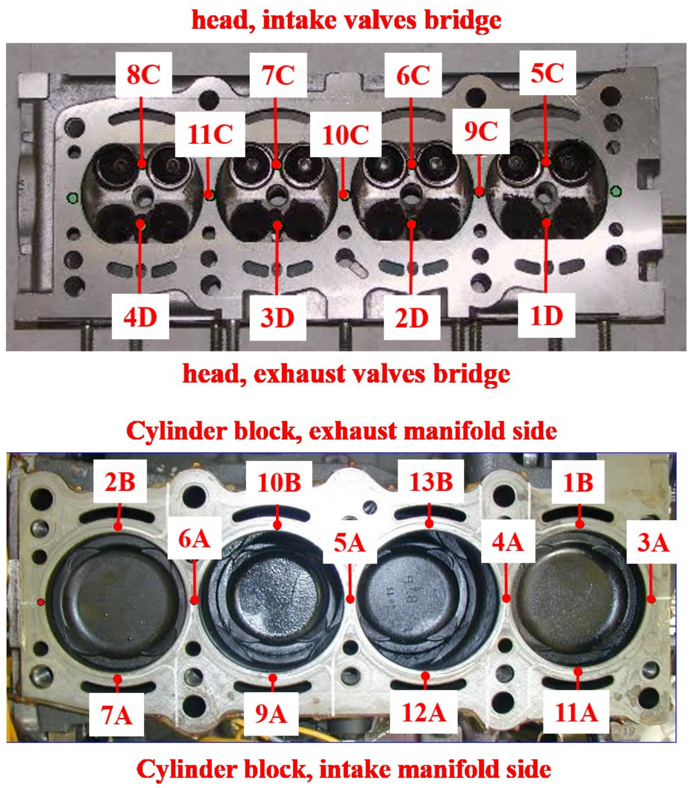

Fig. 2. Thermocouples location in the engine metal.

2.1 Experimental activity

The experimental activity strategies were established in agreement with FGA (Fiat Group Automobiles, now FCA, Fiat Chrysler Automobiles), partner in the framework of the Italian government research project PON01-01517. Seven key-operational conditions were traditionally identified as *canonical points* by the Company; they are defined as (*engine speed)*x(*bmep)* couples of values: 1500x1; 2000x2; 2000x4; 2000x8; 3000x3; 3000x5; 4000x5 (rpm x bar). In this paper the results regarding the condition 2000x2 will be presented. The coolant temperature at the engine inlet was kept constant at the value of 85±1°C. Most of the tests were carried out under steady-state, fully warmed conditions for a sequence of coolant flow rate values, which were varied from a maximum value of 1900 dm^3/h down to 500 dm^3/h. Other tests were conducted under dynamic conditions, by enforcing step variations of coolant flow rate, fuel flow rate or engine speed.

The detection of the onset of nucleate boiling and the identification of the two-phase coolant flow pattern was carried-out by analyzing several physical quantities and was supported by the visual observation of the coolant flow at the transparent window inserted at engine outlet (Fig. 1). In this paper attention was focused on the evolution of the recorded coolant temperature: this quantity was used in order to validate the prevision zero-dimensional model described in the following paragraphs.

Under steady-state, engine fully-warmed conditions, even though the fuel flow rate is kept constant, a reduction in coolant flow rate causes an increase of the engine wall temperature; as a consequence, the heat transfer to the coolant $\dot{Q}_c$ increases and experimental data show that $\dot{Q}_c \propto \left(T_{out} - T_{in}\right)^2$. Under single-phase forced convection regime, both coolant density ρ_c and specific heat c_p are constant in the range of temperature of interest; consequently, as $\dot{Q}_c = \rho_c \dot{V}_c c_p (T_{out} - T_{in})$, $\dot{V}_c \propto (T_{out} - T_{in})$ i.e. the $(T_{out} - T_{in})$ difference will increase linearly as the coolant volumetric flow rate $\dot{V}_c$ diminishes. On the contrary, when the nucleate boiling regime develops, the coolant density diminishes significantly and the $(T_{out} - T_{in})$ difference increases more rapidly as the coolant volumetric flow rate diminishes. Thus, the coolant temperature difference between engine outlet and engine inlet can be used to detect whether nucleate boiling occurs in a series of measurements made under steady-state conditions for different volumetric coolant flow rates, at constant fuel mass flow rate and constant engine-in coolant temperature.

Figure 3 illustrates the difference between engine-out and engine-in coolant temperature as volumetric coolant flow rate was varied from the maximum value of 1900 dm^3/h down to a minimum value of 500 dm^3/h in a sequence of steady-state operations. The results shown in Fig. 3 refer to the engine operational condition of 2000 rpm and 2 bar bmep, with the cooling circuit set up with the standard radiator closed expansion tank. For each flow rate, the reported experimental value is the mean over more than 150 individual measurements. A linear interpolation of the data was carried out for a variable number of data points; the dashed line, which is reported in the figure, is the interpolation over 13 data points (1447 – 1920 dm^3/h) which gave the highest coefficient of determination, value (R^2=0.990). By reducing the coolant flow rate from the initial 1920 dm^3/h value, the coolant temperature first increases linearly which indicates that the heat transfer mechanism is purely convective. In the coolant flow rate range 1450-1550 dm^3/h the coolant temperature starts to increase more than linearly as the coolant flow rate decreases: in this range the onset of nucleate boiling (ONB) occurs (shadow region in Fig. 3). In these conditions, bubbles form at the heated wall, but then they condense and collapse within the bulk flow so that they cannot yet be observed at the transparent window. As the coolant flow diminishes further, the coolant temperature increases considerably and a net presence of bubbles is clearly visible at the transparent window at a 1150 dm^3/h coolant flow rate. As the coolant flow rate is further reduced down to a value of 1050 dm^3/h the fully developed sub-cooled boiling condition establishes, the bulk liquid temperature reaches the saturation temperature (saturated boiling), and a net vapor production is visible at the transparent window (*FBD*). These two flow rates values are indicated by the two vertical dashed lines in Fig. 3. Repeated measurement sequences gave very similar results.

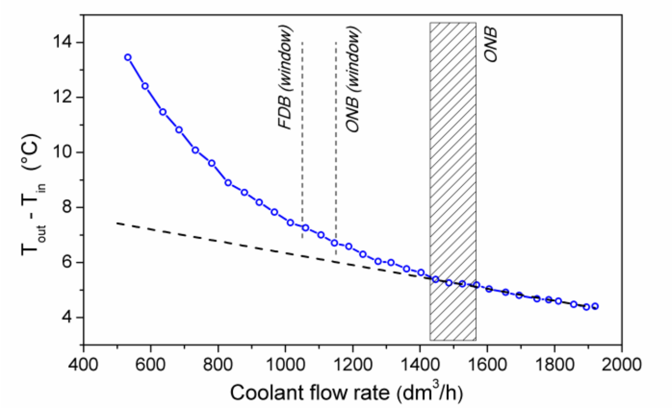

Fig. 3. Coolant temperature increase between engine inlet and outlet as a function of the imposed coolant flow rate. The shadow region indicates the experimental evidence of the Onset of Nucleate Boiling. Vertical dashed lines indicate the Onset of Nucleate Boiling and the Fully developed Boiling regimes respectively as detected through the transparent window. Operational condition: 2000rpm, bmep 2 bar.

2.2 Repeatability analysis

Repeatability analysis is summarized in Table 2, where the results are given in terms of mean value, standard deviation and precision index, U_D, for all the measured variables. U_D is computed as $t \cdot S / \sqrt{N}$ where t is the t-distribution, S is the standard deviation, and N is the number of samples. Experimental tests were repeated for three values of coolant flow rate: 1800, 1400 and 1200 dm^3/h and, for each condition, a minimum of eight repeated tests were carried out.

As for wall temperature, Table 2 includes the value recorded by thermocouple 1D for the sake of simplicity, although the temperatures measured by all the thermocouples were analyzed. These are taken into account through the average wall temperature value over all the thermocouples. In general, a very good repeatability is observed for coolant flow rate as well as for coolant inlet and outlet temperatures, while slightly larger uncertainties are registered for coolant pressure and for wall temperature values.

Table 2
Repeatability analysis

Parameter	**Imposed coolant flow rate (dm^3/h)**	**Number of samples**	**Mean value**	**Standard deviation**	**U_D (% of mean value)**
	1800	8	1778.7	6.1	0.24
Inlet coolant flow rate (dm^3/h)	1400	8	1389.3	21.2	1.08
	1200	8	1189.1	4.7	0.28
	1800	8	85.30	0.42	0.34
Inlet coolant temperature (°C)	1400	8	85.33	0.30	0.25
	1200	8	85.31	0.35	0.29
	1800	8	89.96	0.33	0.26
Outlet coolant temperature (°C)	1400	8	91.08	0.20	0.16
	1200	8	91.93	0.23	0.17
	1800	8	1.62	0.05	2.01
Coolant pressure (bar)	1400	8	1.56	0.04	1.89
	1200	8	1.53	0.05	1.65
	1800	8	146.27	5.31	2.56
Thermocouple 1D (°C)	1400	8	147.69	5.48	2.62
	1200	8	149.19	4.72	2.24
	1800	8	122.09	4.67	2.70
Average Wall Temperature (°C)	1400	8	123.88	4.82	2.75
	1200	8	125.37	4.64	2.62

3. MODEL DESCRIPTION

The cooling system of an ICE is modeled by a zero-dimensional approach, with the aim to simulate the thermal behavior of the cooling system of an SI engine, both in forced convection and nucleate boiling flow regimes. The model focuses, in particular, on the heat exchange between the coolant and the engine walls and is designed in order to predict dynamically the heat transfer mechanism, which occurs within the engine cooling system with varying the engine operating conditions. According to whether forced convection or nucleate boiling occurs, the model makes use of the proper set of equations to compute the exchanged heat flux and then evaluates the instantaneous coolant temperature at engine exit, the space-averaged engine wall temperature and the amount of wall area where nucleate boiling occurs. The required input data are coolant flow rate, engine-in coolant temperature and pressure, fuel flow rate and engine speed (Fig. 4).

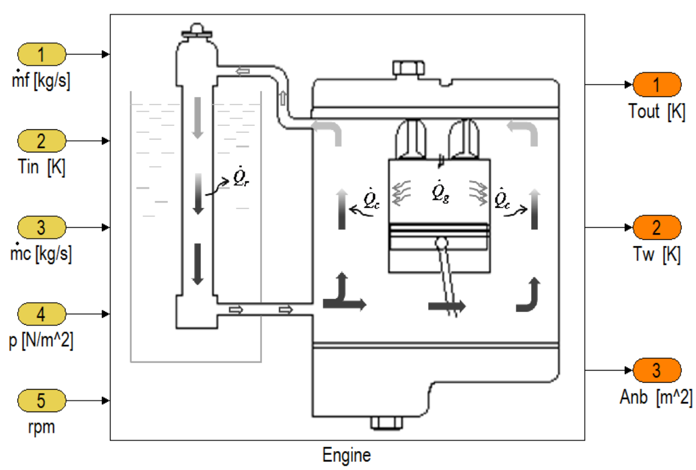

Fig.4 Model input and output variables.

The global parameters used to describe the cooling system characteristics are the engine and coolant thermal capacities, C_w and C_c, respectively and total coolant-metal heat exchange area. These parameters can be easily estimated and the values used for the present investigation are reported in Table 3. Heat losses owing to natural convection and radiation are neglected and it is assumed that the unique source of thermal power to the coolant is the one provided by the fuel. This is estimated by a modified version of the empirical correlation reported in [18], by taking into account fuel flow rate, coolant flow rate and engine speed. The wall-coolant heat exchange in forced convection flow regimes is modeled through the well-known *Dittus-Boelter* correlation [19], whereas the *Chen* approach is used for heat exchange in nucleate boiling flow regimes [20].

The following sections briefly describe the fundamental aspects of the engine wall-coolant heat exchange and introduce the correlations used in the model.

Table 3
Engine data

Parameter	Value/Description
Cylinder Head Material	Aluminum
Crankcase Material	Cast iron
Total Heat Exchange Area	0.10 m^2
Combustion Chamber Thickness	0.012 m
Cylinder Head Area	0.032 m^2
Coolant	Water/Ethyl glycol 50/50 (%vol)
Metal Heat Capacity (C_w)	2.56 kJ/°C
Coolant Heat Capacity (C_c)	32 kJ/°C

3.1 Zero-dimensional model equations

Model input and outputs are shown in Fig. 4. Spatial-averaged wall and coolant temperature, T_w and T_c are obtained by the energy conservation equations:

$$\dot{T}_w C_w = \dot{Q}_g - \dot{Q}_c \qquad (1)$$

$$\dot{T}_c C_c = \dot{Q}_c - \dot{Q}_r \qquad (2)$$

where C_w and C_c are the engine and coolant thermal capacities, respectively, and $\dot{Q}_g$, $\dot{Q}_c$ and $\dot{Q}_r$ are the thermal power transferred by the combustion gases to the engine walls, by the engine walls to the coolant and by the coolant to the radiator respectively. For $\dot{Q}_g$ Heywood [18] proposed an empirical expression which correlates the fuel thermal power to the fuel flow rate, $\dot{m}_f$, through the coefficients c and n:

$$\dot{Q}_g = c(\dot{m}_f)^n \tag{3}$$

In traditional engines, for a fixed load, both fuel and coolant flow rates are determined linearly by engine speed and equation 3 adequately correlates data of different engines. In the present investigation, the use of an electrical pump gives the possibility of varying the coolant flow rate independently of the engine speed. Consequently, in order to take into account the effects of $\dot{m}_c$ and N on $\dot{Q}_g$ separately, equation 3 was modified according to the following formulation:

$$\dot{Q}_g = c \cdot N^{n_1} \dot{m}_c^{\,n_2} (\dot{m}_f)^n \tag{4}$$

where c, n, n_1 and n_2 were estimated through the procedure described in Section 3.4.

The thermal power transferred to the coolant by the engine walls, $\dot{Q}_c$, is computed as:

$$\dot{Q}_c = h_{mac} A(T_w - T_\infty) + h_{mic} A_{nb} (T_w - T_{sat}) \tag{5}$$

The heat exchange is made up of two main contributions: the forced convection and nucleate boiling. In Eq. 5, A is the total heat exchange area, while A_{nb} is the part of the engine walls involved in the nucleate boiling phenomenon. When heat transfer is limited to forced convection only, A_{nb} in Eq. (5) is zero, and a single phase flow regime occurs within the cooling system. The heat transfer coefficients h_{mac} and h_{mic} owing to forced convection and nucleate boiling respectively, are computed according to the procedure, which will be described in the next section (Sec.3.2).

Finally, the thermal power, released by the coolant to the atmosphere through the radiator, is obtained by the following equation:

$$\dot{Q}_r = \dot{m}_c c_p \left(T_{out} - T_{in}\right) \tag{6}$$

where T_{in} , coolant engine-in temperature, is measured and T_{out}, coolant engine-out temperature, is computed by the model.

3.2 Correlations for heat transfer coefficient in nucleate boiling

The governing equations for nucleate boiling heat transfer, which are used in the present model, follow the approach proposed by *Chen* [20]. This approach was originally developed for saturated boiling flows of water inside uniformly heated vertical axial channels. Several modifications were subsequently proposed for practical applications, which differ in definition of some model parameters. *Chen*'s concept is, however, a well-established approach for practical engineering applications and considers two basic mechanisms that take part in the total heat transfer: the ordinary macro-convection and the micro-convection associated with bubble nucleation, growth and detachment. The local heat flux is, then, given by the sum of these contributions according to the following expression:

$$q_w = h_{mac}\left(T_w - T_\infty\right) + h_{mic}\left(T_w - T_{sat}\right) \tag{7}$$

Considering first the macro-convection term, T_w-T_∞ is the difference between wall and bulk flow temperatures and the heat transfer coefficient and h_{mac} is computed by the *Dittus-Boelter* heat transfer coefficient for single phase flows, h_{fc}, by a multiplying factor F, which takes into account the presence of bubbles in the bulk flow:

$$h_{mac} = F \cdot h_{fc} \tag{8}$$

The *Dittus-Boelter* correlation for the liquid phase flow gives [19]:

$$h_{fc} = 0.023 \cdot \mathrm{Re}_l^{0.8} \cdot \mathrm{Pr}_l^{0.4} \cdot \frac{k_l}{L} \tag{9}$$

This correlation is valid for fully developed turbulent flows within heated circular cylinders. In Eq.(9) the characteristic length, L, is given by the hydraulic diameter of the coolant ducts within the engine and the correction factor, F, is:

$$F = \left(1 + X_{tt}^{-0.5}\right)^{1.78} \tag{10}$$

It takes into account the enhanced convective heat transfer due to vapor bubble agitation and depends on the amount of vapor fraction, x, through the Martinelli parameter, X_{tt}:

$$X_{tt} = \left(\frac{1-x}{x}\right)^{0.9} \cdot \left(\frac{\rho_g}{\rho_l}\right)^{0.5} \cdot \left(\frac{\mu_l}{\mu_g}\right)^{0.1} \tag{11}$$

The subscripts l and g refer to the liquid and gas phases, respectively. For small vapor fractions associated with $1/X_{tt} < 0.1$, F can be assumed equal to 1.

The second term of Eq.7 refers to the nucleate boiling heat exchange and T_w-T_{sat} is the difference between wall and flow saturation temperature. The micro-convective coefficient, h_{mic}, is obtained from the *Foster* and *Zuber* correlation for pool boiling [10], modified by Chen [20] in order to take into account the effects of the flow velocity, through a suppression factor S. Therefore:

$$h_{mic} = S \cdot h_{nb} \tag{12}$$

The *Foster and Zuber* coefficient, h_{nb}, is given by:

$$h_{nb} = 0.00122 \cdot \left(\frac{k_l^{0.79} \cdot c_{pl}^{0.45} \cdot \rho_l^{0.49}}{\sigma^{0.5} \cdot \mu_l^{0.29} \cdot h_{\lg}^{0.24} \cdot \rho_g^{0.24}}\right) \cdot \Delta T_{sat}^{0.24} \cdot \Delta p_{sat}^{0.75} \tag{13}$$

where ΔT_{sat} is the difference between the wall temperature and saturation temperature; Δp_{sat} is the difference between the vapor pressure corresponding to the wall temperature, p_w, and the bulk flow saturation pressure, with p_w given by the Antoine correlation for vapor pressure [21]:

$$p_w = 133.32 e^{E} \tag{14}$$

and

$$E = 18.3036 - \left(\frac{3816.44}{T_w - 46.13} \right) \tag{15}$$

Finally, the suppression factor, *S,* which considers the effects of flow velocity on nucleate boiling, depends on the two phase Reynolds number (Re_{2ph}) and takes into account the observed reduction of nucleate boiling as the flow velocity increases. The multiplying factor *S* was determined empirically from experimental data, and a graphical solution as a function of (Re_{2ph}) was given by Chen. Several analytical best fitting formulations were then proposed for *S*. Herein, the formulation proposed by *Kreith* and *Bohn* [22] is used:

$$S = \begin{cases} \dfrac{1}{1 + 0.12 \cdot \mathrm{Re}_{2ph}^{1.14}} & \mathrm{Re}_{2ph} < 32.5 \\ \dfrac{1}{1 + 0.42 \cdot \mathrm{Re}_{2ph}^{0.78}} & 32.5 < \mathrm{Re}_{2ph} < 70 \\ 0.1 \quad \mathrm{Re}_{2ph} > 70 & \end{cases} \tag{16}$$

where Re_{2ph} is computed as:

$$\mathrm{Re}_{2ph} = \mathrm{Re}_l \cdot F^{1.25} \cdot 10^{-4} \tag{17}$$

3.3 Prediction of the onset of nucleate boiling

The correlation developed by *Frost* and *Dzakowic* (1967) [23], which is valid for a wide variety of liquids, is adopted for predicting the onset of nucleate boiling within the cooling system of the tested SI engine. In a typical subcooled flow, the formation of vapor bubbles starts, after the wall temperature has reached the saturation temperature, at T_{ONB} (Fig. 5, [11]). According to Frost and Dzackowich [23], the temperature difference ΔT_{sat} between wall and coolant required for the onset of nucleate boiling, is given by:

$$(\Delta T_{sat})_{ONB} = (T_w - T_{sat})_{ONB} = X \Pr_l q_w^{0.5} \tag{18}$$

where X is a parameter determined by the fluid physical properties and is computed as:

$$X = \left[\frac{8\sigma T_{sat}}{J h_{lg} k_l \rho_g} \right]^{0.5} \tag{19}$$

and q_w denotes the heat flux through the walls. The heat flux needed for the onset of nucleate boiling can be computed by the heat transfer equation for subcooled boiling region as:

$$q_{ONB} = h_{fc} \left((\Delta T_{sat})_{ONB} + (T_{sat} - T_\infty) \right) \tag{20}$$

In order to compute both the heat flux, q_{ONB}, and the wall temperature, T_{ONB}, needed for the onset of nucleate boiling, Eq.(18) and Eq. (20) must be solved simultaneously.

If the actual thermal flux, q_w, is higher than the needed one, q_{ONB}, then nucleate boiling occurs and the nucleate boiling area, A_{nb}, which is used in Eq. 5 for the estimation of the thermal power removed by the coolant, is computed as a percentage of the total heat exchange surface, A, as:

$$\begin{cases} A_{nb} = \dfrac{(q_w - q_{ONB})}{q_w} \cdot A & q_w > q_{ONB} \\ \\ A_{nb} = 0 & q_w \le q_{ONB} \end{cases} \tag{21}$$

On the contrary, if the actual thermal flux is lower than the needed one, A_{nb} in Eq.5 is set to zero and the cooling action is due to forced convection only.

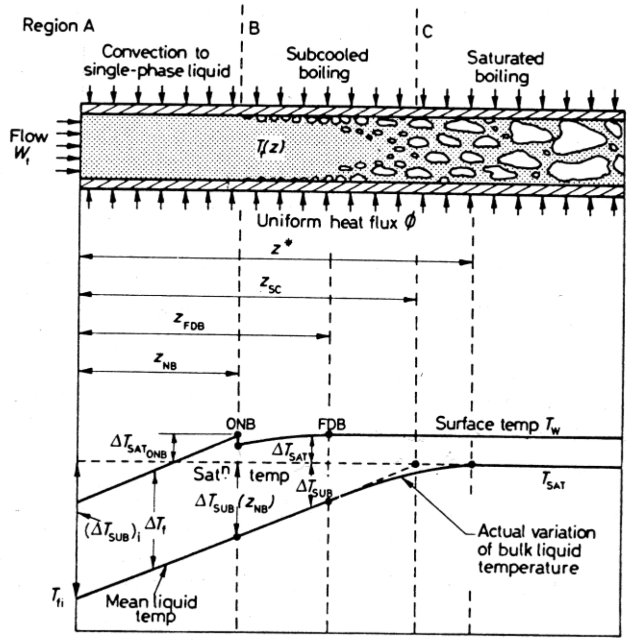

Fig.5 Flow in a uniformly heated pipe. Wall temperatures and liquid temperatures variations along the flow direction. Onset of nucleate boiling conditions are marked by ONB [11].

3.4 Model calibration

The coefficients c, n, n_1 and n_2 in Eq.4 were estimated under steady-state conditions by assuming that the thermal power transferred from the combustion hot gasses to the engine walls is equal to the one removed by the coolant:

$$\dot{Q}_g = \dot{Q}_c \tag{22}$$

The thermal power supplied to the coolant, $\dot{Q}_c$, is obtained experimentally by measuring engine-in, engine-out coolant temperature and coolant mass flow rate T_{in}, T_{out} and $\dot{m}_c$. A suitable interpolation algorithm then provides the c, n_1 and n_2 coefficients from the following relationship:

$$c \cdot N^{n_1} \dot{m}_c^{\,n_2} \left(\dot{m}_f\right)^n = \dot{m}_c c_p \left(T_{out} - T_{in}\right) \tag{23}$$

4. RESULTS

The model was validated under several operating conditions, which include variations in coolant flow rate, engine speed and bmep. The results are presented in the following paragraphs.

4.1 Coolant flow rate variation

Experimental tests were carried out by reducing the coolant flow rate as a sequence of steady state conditions, at fixed engine speed and bmep (2000 rpm, 2 bar). Figure 6 includes the experimental coolant temperature increase between engine inlet and outlet (top), the experimental coolant pressure (middle) and the nucleate boiling area predicted by the model (bottom) as a function of the imposed coolant flow rate. The behavior of coolant temperature increase (T_{out}-T_{in}) has been described in paragraph 2.1. Coolant pressure for fired and switched-off engine is reported in Fig.6 (middle). In both operational conditions, coolant temperatures are similar. As coolant flow rate is reduced, coolant pressure diminishes owing to the pump head decrease. The behavior is the same in the two engine conditions. However, for coolant flow rates lower than ~1400-1500 dm^3/h, for switched-off condition the coolant pressure still decreases, while during the normal engine operation it reverses the trend. This is due to the production of vapor. Therefore, the experimental data indicate that the nucleate boiling starts at a coolant flow rate in the range of 1550 ± 50 dm^3/h, with an uncertainty of about 3%. According to the model (Fig.6 bottom), at high coolant flow rates, the heat transfer mechanism is purely convective (nucleate boiling Area=0) and the onset of nucleate boiling occurs about 1550 dm^3/h. Figure 7 shows the total heat exchange coefficient $h_{tot} = h_{mac} + h_{mic}$. The figure clearly illustrates that in the single phase regime the heat transfer coefficient diminishes as the coolant flow rate is reduced; it suddenly increases during the single phase – boiling transition and then reaches a value (7-8000 $W/m^2/K$) which is about one order of magnitude higher than the ones available in the single phase regime.

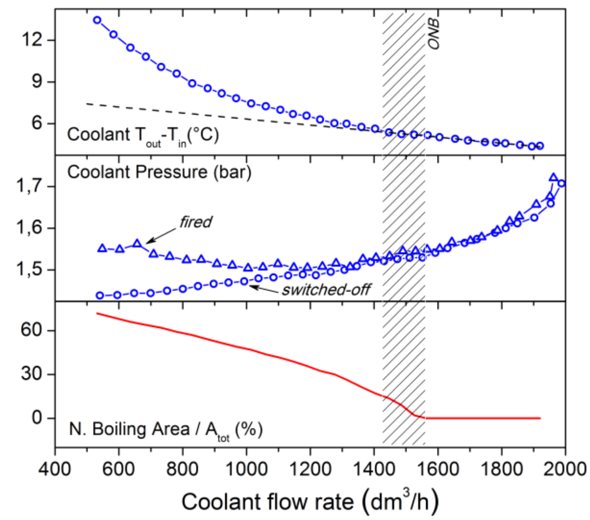

Fig.6 Experimental coolant temperature increase (top) and experimental coolant pressure both in fired and switched-off engine operational condition (middle) as a function of coolant flow rate in a sequence of steady-state conditions. Model estimation of the nucleate boiling area as % of the total heat exchange area (bottom). Dashed area indicates the Onset of Nucleate Boiling (ONB). Operational condition: 2000 rpm, bmep=2 bar.

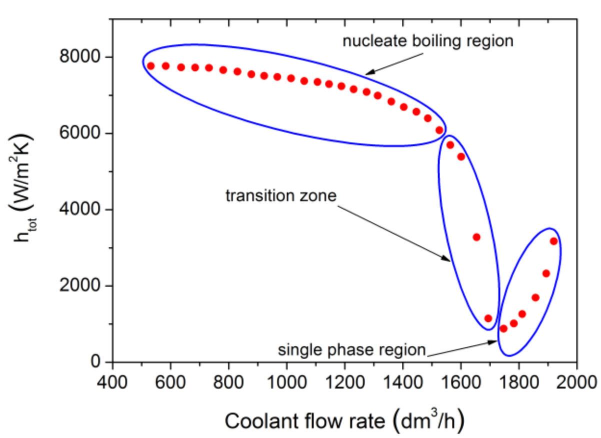

Fig.7 Total heat exchange coefficient (W/m^2K) predicted by the model. Operational condition: 2000 rpm, bmep=2bar, coolant flow rate reduction.

The model also predicts the other experimental quantities well. Fig. 8 shows the predicted engine-out coolant temperature compared to the experimental data. The average error amounts to 0.4 %. The comparison between experimental and predicted engine wall temperature is plotted in Fig. 9. The model calculates a spatial-averaged wall temperature value, while the experimental data are average values over the temperatures recorded both in the engine head and in the cylinder block, very close to the gasket. The model predicted temperatures are quite good agreement with the experimental averaged values as long as single phase and nucleate boiling regimes occur; when fully developed boiling is observed, the divergence increases, as this regime is not modeled.

Finally, Figure 10 summarizes the overall power balance, by showing the thermal power entering with the fuel, the brake power and the thermal power delivered to the coolant. This last quantity is compared with the thermal power delivered to the engine wall by the fuel, as predicted by the proposed model (eq. 4). The agreement is very satisfactory, with an average error of 7%. As the fuel mass flow rate is kept constant, the total power entering the engine and brake power are constant. On the contrary, the thermal power delivered by the fuel to the wall diminishes as a result of wall temperature increase.

A further experimental campaign was carried out by enforcing a step variation of the coolant flow rate (Fig. 11, top). The coolant pressure, which is expected to increase as the coolant flow rate increases, shows a steady behavior despite the flow rate change. This is the consequence of two opposite contributions: on one hand, the pressure tends to increase due to the pump head, on the other hand the pressure decreases due to the mass reduction of coolant vapor, which occurs at the coolant flow rate step. The predicted nucleate boiling area variation as a consequence of the coolant flow rate shows that the transition from nucleate boiling heat transfer to forced single-phase convection is well predicted.

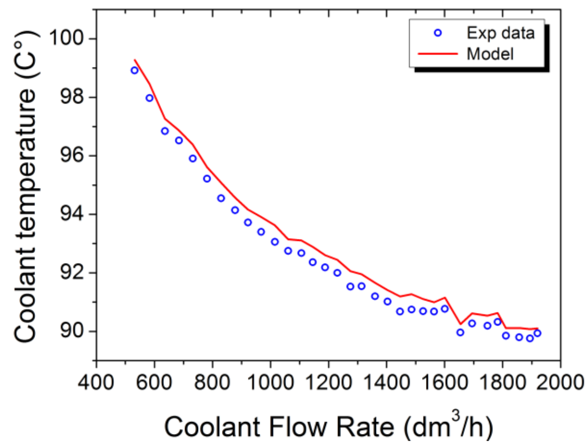

Fig.8 Experimental engine-out coolant temperature as a function of coolant flow rate in a sequence of steady-state conditions and model prediction. Operational condition: 2000 rpm, bmep=2 bar.

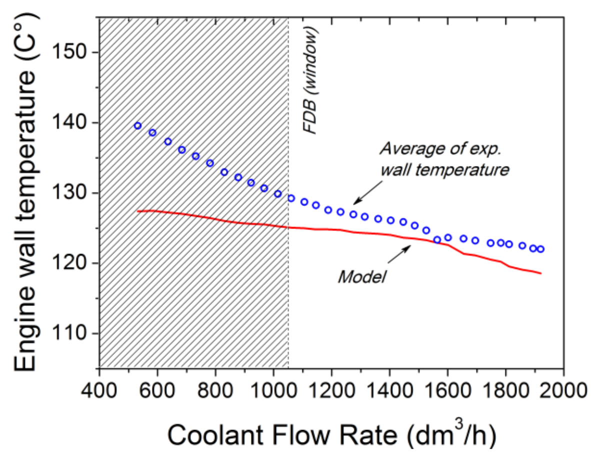

Fig.9 Wall temperatures as a function of coolant flow rate in a sequence of steady-state conditions. The experimental curve is obtained as average of the values recorded by all the thermocouples located at the engine head and cylinder block. The dashed area indicates the Fully Developed Boiling flow regime. Operational condition: 2000 rpm, bmep=2 bar.

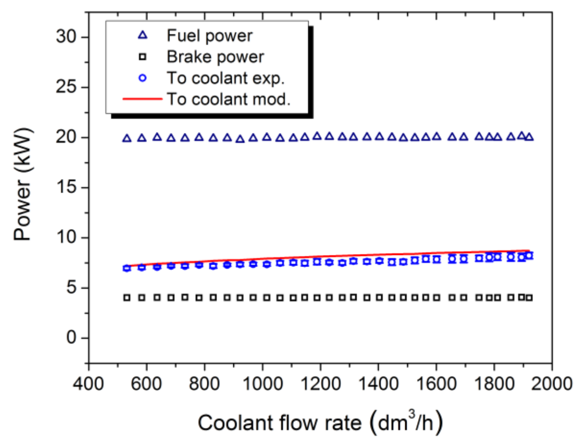

Fig.10 Overall power balance for engine operational conditions 2000 rpm, bmep=2 bar, as coolant flow rate is reduced.

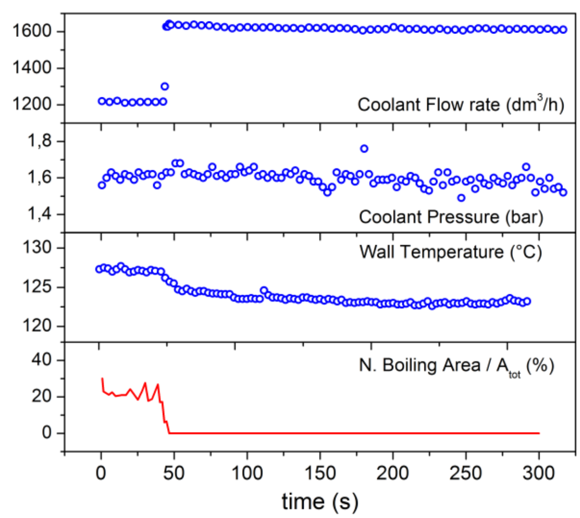

Fig.11 Experimental coolant flow rate step variation (1210 dm^3/h to 1640 dm^3/h). Experimental time history of coolant pressure and average wall temperature. Predicted nucleate boiling area as % of the total heat exchange area (bottom). Operational condition: 2000 rpm, bmep=2 bar.

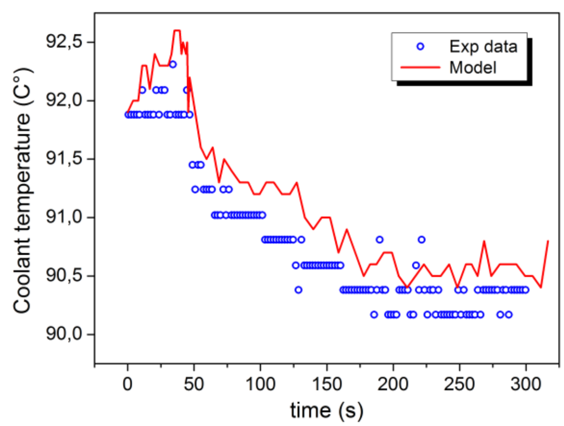

Fig.12 Experimental and predicted time histories of engine-out coolant temperature at operational conditions involving coolant flow rate step variation. Operational condition: 2000 rpm, bmep=2 bar.

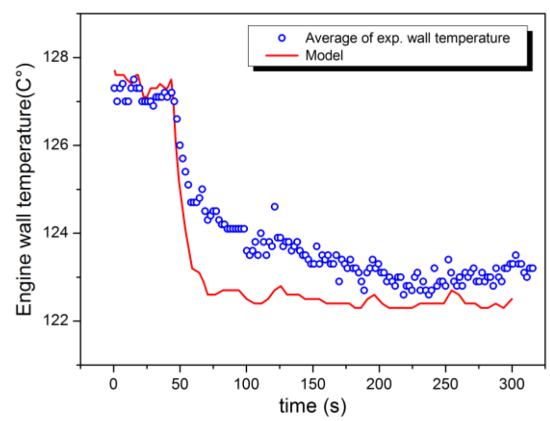

Fig.13 Wall average temperatures at engine operational conditions involving coolant flow rate step variation. Operational condition: 2000 rpm, bmep=2 bar.

Figures 12 and 13 present the comparison of experimental and predicted engine-out coolant temperature and engine wall averaged temperatures, respectively. The dynamic behavior of coolant temperature is once again well captured (average error 0.35%), while the model predicts a faster transition of the wall temperature with respect to the experiments. This is due thermal inertia of the lubricant, which in not taken into account.

4.2 Engine speed variation

This sub-section presents the results of tests where the engine speed is varied in a sequence of steps. In this case both engine speed and fuel flow rate increase, while the coolant flow rate and throttle position are kept constant (1600 dm^3/h; bmep about 2 bar). Figure 14 shows that the nucleate boiling already starts at 2500 rpm, as shown by the nucleate boiling area values. As expected, the wall temperature increases at each engine speed step due to the increase of the fuel flow rate. As engine speed further increases, the bubbles development and implosions process causes coolant pressure oscillations. Owing to the increased wall temperature, the engine-out coolant temperature augments as well, as depicted in Fig. 15. This coolant temperature is well predicted by the model both in values and in dynamic behavior (average error 0.41%).

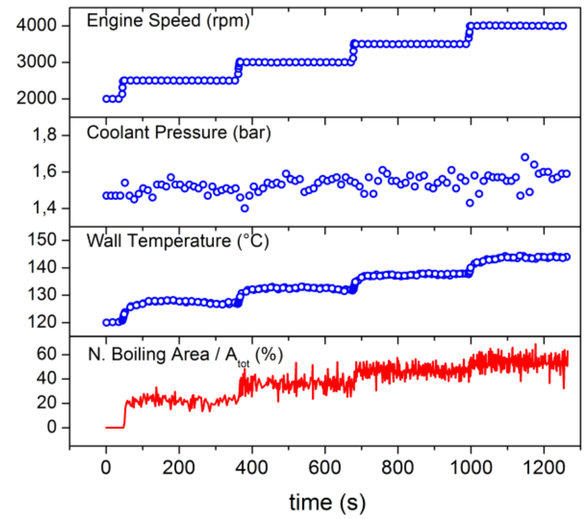

Fig.14 Engine speed variation in a sequence of steps. Experimental time history of coolant pressure and of wall average temperature. Predicted nucleate boiling area as % of the total heat exchange area (bottom). Coolant flow rate 1600 dm^3/h; bmep about 2 bar.

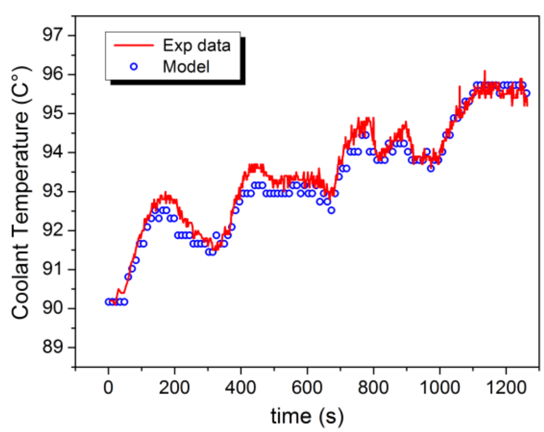

Fig.15 Time history of engine-out coolant temperature at operational conditions involving steps of engine speed variation. Comparison between model prediction and experimental data. Coolant flow rate 1600 dm^3/h; bmep about 2 bar.

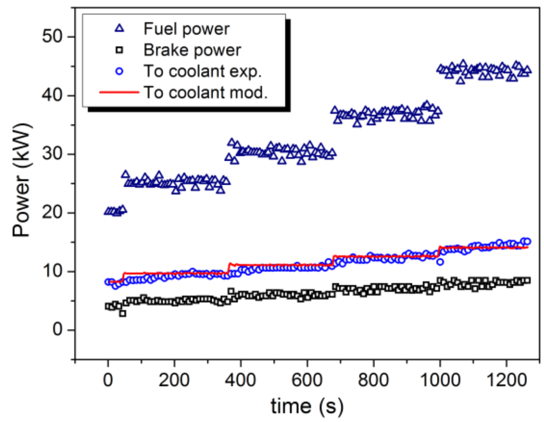

Fig.16 Overall power balance for engine operational conditions involving step engine speed variations. Coolant flow rate 1600 dm^3/h; bmep about 2 bar.

Finally, Fig. 16 shows the total thermal power entering with the fuel, the brake power, the thermal power delivered by the fuel to the engine wall, as predicted by the model, and the thermal power transferred by the wall to the coolant. The proposed model gives a quite good estimation of the thermal power delivered by the fuel to the walls.

4.3 Bmep variation

The last experimental campaign was carried out by the enforcement of a bmep step variation, from 2 to 4 bar, while the engine speed and the coolant flow rate were kept constant (2000 rpm, 1600 dm^3/h). The model predicts the onset of nucleate boiling at the bmep step, as shown in Fig. 17. As expected, the engine wall temperature varies accordingly and shows an increase due to the fuel mass flow rate rise. Figure 18 shows the engine-out coolant temperature variation as a result of the step fuel flow rate rise. The model well predicts the temperature behavior, both in terms of absolute values and of dynamic response.

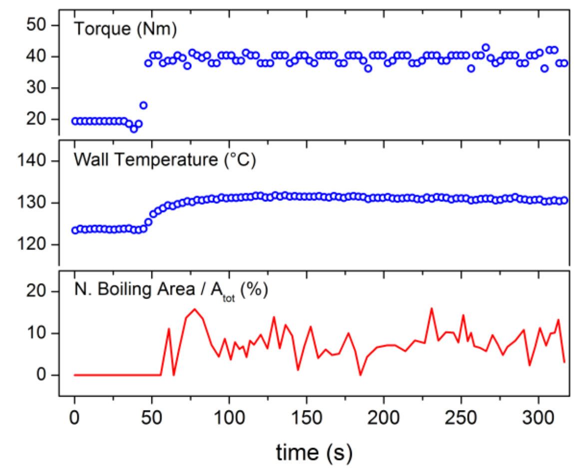

Fig.17 Bmep step variation (top), experimental time history of wall average temperature (middle) and predicted nucleate boiling area as % of the total heat exchange area (bottom). Operating conditions: 2000 rpm, 1600 dm^3/h coolant flow rate.

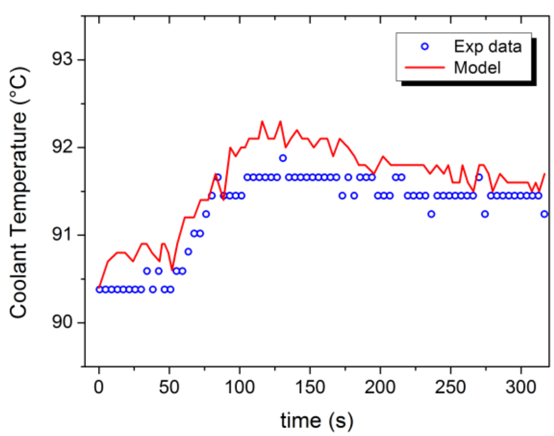

Fig. 18 Experimental and predicted engine-out coolant temperature time history as a result of the bmep step enforcement. Operating conditions: 2000 rpm, 1600 dm^3/h coolant flow rate.

5. SUMMARY AND CONCLUSIONS

An original zero-dimensional dynamic model of the cooling system of an internal combustion engine was developed, which is able to operate both under single-phase and nucleate boiling conditions. The model is able to predict metal temperature, coolant temperature and fraction of wall metal area, which is subjected to nucleate boiling. The comparison with experimental data obtained under varying conditions of coolant flow rate, engine speed and fuel flow rate exhibited good agreement.

As an experimental detection of nucleate boiling on-set is not feasible on-board of a vehicle, the model can be used conveniently in cooling control strategies in order to set-up the optimal flow rate. This optimal value will change depending on the desired goal. If the objective is the fastest possible warm-up (cold-start conditions), the controller will correct the actual flow in order to maintain the single-phase flow regime, with the lowest possible heat transfer coefficient. On the contrary, under fully warmed condition, the controller will update the actual flow rate, until the model will yield a small but positive nucleate boiling area. In such a way, a higher heat transfer coefficient combined with a small fraction of wall surface that operates under nucleate conditions, will be obtained, therefore preserving engine reliability.

The adoption of adequate cooling control strategies will result in lower fuel consumption and reduced CO_2 emissions. Although no data has been published yet, it is widely recognized among car manufacturers that a 100 s quicker warm-up produces a reduction of ≈1% in fuel consumption and, consequently, in CO_2 emission along the NEDC for a small-medium weight car.

6. ACKNOWLEDGEMENTS

The investigation was funded by the Italian Ministry of University and Research under the project PON01_01517, CUP: B21H11000400005, with financial support of the European Commission.

REFERENCES

1. EC. Setting emission performance standards for new passenger cars as part of the community's integrated approach to reduce CO2 emissions from light-duty vehicles, No. 443/2009, Off J Eur Union, 2009.

2. Bishop, J., Martin, N., Boies, A. Cost-effectiveness of alternative powertrains for reduced energy use and CO_2 emissions in passenger vehicles. Appl. Energ. 2014; 124: 44-61.

3. Silva, C., Ross, M., Farias, T. Analysis and simulation of ‘‘low-cost” strategies to reduce fuel consumption and emissions in conventional gasoline light-duty vehicles. Energ. Convers. Manage. 2009; 50(2):215–222. DOI:10.1016/j.enconman.2008.09.046.

4. Johnson, T. Vehicular Emissions in Review. SAE Int. J. Engines 2012; 5(2):216-234. DOI:10.4271/2012-01-0368.

5. Clough, M. Precision Cooling of a Four Valve per Cylinder Engine. SAE Technical Paper 931123, 1993. DOI:10.4271/931123.

6. Bova, S., Piccione, R., Durante D., Perrussio, M. Experimental Analysis of the After-Boiling Phenomenon in a Small I.C.E. SAE Technical Paper 2004-32-0091, 2004. DOI:10.4271/2004-32-0091.

7. Piccione, R., Bova, S. Engine Rapid Shutdown: Experimental Investigation on the Cooling System Transient Response, J. Eng. Gas. Turb. Power 2010; 132(7), 072801:1-10. DOI: 10.1115/1.4000262.

8. Rohsenow, W.M. A method of correlating heat transfer data for surface boiling of liquids, J. Heat Transfer Trans. ASME 1952; 74:969–976.

9. Engelberg-Forster, K. and Greif, R. Heat transfer to a boiling liquid – mechanism and correlations, J. Heat Transfer Trans. ASME 1959; 81:43–53.

10. Foster, H.K. and Zuber, N. Dynamics of Vapor Bubbles and Boiling Heat Transfer. AIChE Journal 1955; 1(4):531-535. DOI:10.1002/aic.690010425.

11. Collier, J. and Thome, R. Convective Boiling and Condensation, Oxford University Press, New York, 1994.

12. Sanna, A. , Hutter, C., Kenning, D.B.R., Karayiannis, T.G., Sefiane, K., Nelson, R.A. Numerical investigation of nucleate boiling heat transfer on thin substrates, Int. J. Heat Mass Tran. 2014; 76:45–64. DOI:10.1016/j.ijheatmasstransfer.2014.04.026.

13. Pretscher, M. and Ap, N.S. Nucleate Boiling Engine Cooling System – Vehicle Study, SAE Technical Paper 931132, 1993. DOI:10.4271/931132.

14. Ap, N. and Golm, N. New Concept of Engine Cooling System (Newcool). SAE Technical Paper 971775, 1997. DOI:10.4271/971775.

15. Robinson, K., Campbell, N.A.F., Hawley, J.G., Tilley, D.G. A Review of Precision Cooling. SAE Technical Paper 1999-01-0578, 1999. DOI:10.4271/1999-01-0578.

16. Brace, C.J., Burnham-Slipper, H., Wijetunge, R.S., Vaughan, N.D., Wright, K., Blight, D. Integrated Cooling System for Passenger Vehicles. SAE Technical Paper 2001-01-1248, 2001.

17. Amelio, M., Barbara, F., Bova, S., Oliva, P. Experimental Investigation on an ICE Cooling System under Nucleate Boiling Conditions. SAE Technical Paper 2001-01-1795, 2001. DOI: 10.4271/2001-01-1795.

18. Heywood, J.B., Internal Combustion Engine Fundamentals, McGraw-Hill, New York, 1988.

19. Dittus, F.W. and Boelter, L.M.K. Heat Transfer in Automobile Radiators of the Tubular Type. Univ. Calif. Publ. Eng. 1930; 2:443-461.

20. Chen, J.C. Correlation for Boiling Heat Transfer to Saturated Fluids in Convective Flow. Ind. Eng. Chem. Process Des. Dev. 1966; 5(3):233-329. DOI: 10.1021/i260019a023.

21. Reid, R.C., Prausnitz, J.M., Poling, B.E. The Properties of Gases and Liquids. McGrawHill, 1987.

22. Kreith, F. and Bohn, M.S. Principles of Heat Transfer, Harper and Row, 1986.

23. Frost, W and Dzackovic, G.S. An Extension of the Method of Predicting Incipient Boiling on Commercially Finished Surfaces. ASME-AIChE Heat Transfer Conference, 1967, 67-HT-61.

FIGURES CAPTIONS

Fig.1 Schematic of the test rig.

Fig.2 Thermocouples location in the engine metal.

Fig.3 Coolant temperature increase between engine inlet and outlet as a function of the imposed coolant flow rate. The shadow region indicates the experimental evidence of the Onset of Nucleate Boiling. Vertical dashed lines indicate the Onset of Nucleate Boiling and the Fully developed Boiling regimes respectively as detected through the transparent window. Operational condition: 2000rpm, bmep 2 bar.

Fig.4 Model input and output variables.

Fig.5 Flow in a uniformly heated pipe. Wall temperatures and liquid temperatures variations along the flow direction. Onset of nucleate boiling conditions are marked by ONB [11].

Fig.6 Experimental coolant temperature increase (top) and experimental coolant pressure both in fired and switched-off engine operational condition (middle) as a function of coolant flow rate in a sequence of steady-state conditions. Model estimation of the nucleate boiling area as % of the total heat exchange area (bottom). Dashed area indicates the Onset of Nucleate Boiling (ONB). Operational condition: 2000 rpm, bmep=2 bar.

Fig.7 Total heat exchange coefficient (W/m^2K) predicted by the model. Operational condition: 2000 rpm, bmep=2bar, coolant flow rate reduction.

Fig.8 Experimental engine-out coolant temperature as a function of coolant flow rate in a sequence of steady-state conditions and model prediction. Operational condition: 2000 rpm, bmep=2 bar.

Fig.9 Wall temperatures as a function of coolant flow rate in a sequence of steady-state conditions. The experimental curve is obtained as average of the values recorded by all the thermocouples located at the engine head and cylinder block. The dashed area indicates the Fully Developed Boiling flow regime. Operational condition: 2000 rpm, bmep=2 bar.

Fig.10 Overall power balance for engine operational conditions 2000 rpm, bmep=2 bar, as coolant flow rate is reduced.

Fig.11 Experimental coolant flow rate step variation (1210 dm3/h to 1640 dm3/h). Experimental time history of coolant pressure and average wall temperature. Predicted nucleate boiling area as % of the total heat exchange area (bottom). Operational condition: 2000 rpm, bmep=2 bar.

Fig.12 Experimental and predicted time histories of engine-out coolant temperature at operational conditions involving coolant flow rate step variation. Operational condition: 2000 rpm, bmep=2 bar.

Fig.13 Wall average temperatures at engine operational conditions involving coolant flow rate step variation. Operational condition: 2000 rpm, bmep=2 bar.

Fig.14 Engine speed variation in a sequence of steps. Experimental time history of coolant pressure and of wall average temperature. Predicted nucleate boiling area as % of the total heat exchange area (bottom). Coolant flow rate 1600 dm3/h; bmep about 2 bar.

Fig.15 Time history of engine-out coolant temperature at operational conditions involving steps of engine speed variation. Comparison between model prediction and experimental data. Coolant flow rate 1600 dm3/h; bmep about 2 bar.

Fig.16 Overall power balance for engine operational conditions involving step engine speed variations. Coolant flow rate 1600 dm3/h; bmep about 2 bar.

Fig.17 Bmep step variation (top), experimental time history of wall average temperature (middle) and predicted nucleate boiling area as % of the total heat exchange area (bottom). Operating conditions: 2000 rpm, 1600 dm3/h coolant flow rate.

Fig. 18 Experimental and predicted engine-out coolant temperature time history as a result of the bmep step enforcement. Operating conditions: 2000 rpm, 1600 dm3/h coolant flow rate.

TABLE CAPTIONS

Table 1 Main measurement devices specifications.

Table 2 Repeatability analysis.

Table 3 Engine data